ARTICLE

$Na_2Fe(SO_4)_2$: an anhydrous 3.6 V, low cost and good safety cathode for rechargeable sodium-ion battery

Received 00th January 20xx,
Accepted 00th January 20xx

DOI: 10.1039/x0xx00000x

Wenli Pan,[a] Wenhao Guan,[a] Shuangyu Liu, [b] Ben Bin Xu,[c] Chu Liang,[d] Hongge Pan,[a] Mi Yan,[a] and Yinzhu Jiang *[a]

Iron-based sulfate cathode materials are promising for rechargeable batteries due to their elevated operating voltages and earth-abundant elemental composition. However, the inherent unstable SO_4^{2-} units in those sulfate materials result in their low-temperature decomposition (<450 °C) and lead to SO_2 gas evolution, which would hinder sulfate electrodes from outputting high voltage in safety. Herein, a new alluaudite-type sulfate cathode $Na_2Fe(SO_4)_2$ for sodium-ion battery is reported, which displays a high operating voltage at ~3.6 V based on Fe^{2+}/Fe^{3+} redox couple as well as superior thermal stability (~580 °C). In both air and inert ambient, its SO_4^{2-} units demonstrate high thermal stability, assuring good safety for battery application. Furthermore, the $Na_2Fe(SO_4)_2$ cathode material shows superior stability toward moisture for easy handling. The cathode exhibits a reversible capacity of 82 mAh g^{-1} at 0.1 C under nonoptimal carbon coating and maintains over 60% capacity retention at 2 C. The excellent sodium storage ability at 0 °C and 55 °C further demonstrates the advantages of $Na_2Fe(SO_4)_2$ for future energy storage applications in a wide temperature range. The present exploration on $Na_2Fe(SO_4)_2$ for sodium-ion battery can pave the way for developing low cost sulfate cathodes combining high voltage and good safety.

Introduction

Lithium-ion batteries (LIBs) have been successfully commercialized as power sources for portable electronics and electric vehicles due to the advantages of high energy density, good rate capability and long cycle life.[1,2] Along with the increasing demands for LIBs, the prime cost is predicted to be driven up by the shortage and the uneven distribution of lithium and some scarce but essential transition metal used in cathodes, such as cobalt.[3-5] On the other hand, the electric energy storage (EES) for renewable sources and grid balancing are highly demanded, where sustainable and low-cost battery technology is desirable to satisfy these emerging applications.[6-8] As a low-cost alternative to LIBs, sodium-ion batteries (SIBs) have recaptured much attention in consideration of abundant resources of sodium and similar chemistry as lithium.[9] Developing cathode materials using earth-abundant element such as iron, could further strengthen the merits of low-cost and sustainability of SIBs.[10]

As the representative of Fe-based cathode materials, $LiFePO_4$ (LFP) has made great commercial success in LIBs.[11-13] However, to some extent, its low voltage plateau (3.4 V) has impeded the improvement of energy density of LFP-based LIBs, which becomes even worse considering the higher standard electrode potential of Na/Na^+ (-2.71 V) as compared to that of Li/Li^+ (-3.04 V).[14] Introducing sulfate radical with stronger inductive effect in Fe-based cathode materials have been demonstrated to be an effective strategy to elevate the operating voltage.[15,16] Yamada *et.al* reported a high operating voltage of ~3.8 V in $Na_2Fe_2(SO_4)_3$, dramatically drawing attention to Fe-based sulfate cathodes for SIBs.[17] After that, other sulfate hydrate cathodes have also been investigated with relative lower voltage but still higher than 3.2 V, such as $Na_2Fe(SO_4)_2{\cdot}4H_2O$ (3.3 V) and $Na_2Fe(SO_4)_2{\cdot}2H_2O$ (3.25 V), proving sulfates as promising high voltage cathode materials.[18,19] However, these reported Fe-based sulfates are still facing some severe difficulties that might hinder the practical applications in SIBs. The sulfate radical in these materials is generally unstable above 450 °C and prone to release SO_2 gas, which probably causes safety issues in practical applications.[17,20,21] On the other hand, the hygroscopicity of sulfate radical makes it necessary for these sulfate materials to be carefully handled in dry environments during synthesis and preservation. In case the hydrates come into being, the crystal structure and the corresponding electrochemical performance of original sulfate cathodes might be deteriorated.[17-19] What is worse, the water that sulfates absorb might aggravate the side reactions between the electrolyte and the electrode, which probably causes irreversible capacity.[22-25] Therefore, it will be worthwhile but challenging to explore Fe-based sulfate combining desirable operating voltage, high thermal stability and superior moisture resistance.

Herein, we report a 3.6 V Fe-based sulfate cathode, $Na_2Fe(SO_4)_2$, exhibiting outstanding thermal stability and favorable moisture-resistant property. Unlike the previously reported sulfate cathodes

[a] State Key Laboratory of Silicon Materials, Key Laboratory of Novel Materials for Information Technology of Zhejiang Province and School of Materials Science and Engineering, Zhejiang University, Hangzhou, Zhejiang 310027, P. R. China.
[b] State Key Laboratory of Advanced Transmission Technology, Global Energy Interconnection Research Institute Co. Ltd, Beijing 102211, China.
[c] Smart Materials and Surfaces Lab, Mechanical Engineering, Faculty of Engineering and Environment, Northumbria University, Newcastle upon Tyne NE1 8ST, UK
[d] College of Materials Science and Engineering, Zhejiang University of Technology, Hangzhou, Zhejiang 310014, PR China
†Electronic Supplementary Information (ESI) available. See DOI: 10.1039/x0xx00000x

that are prone to decompose and release SO_2 gas above 400 °C, $Na_2Fe(SO_4)_2$ is thermally stable without gas evolution up to 580 °C, assuring good safety for the practical applications. Furthermore, no hydrate forms and both its structure and capacity remain almost unchanged upon exposed to air ambient for 60 days, demonstrating the superior moisture resistance of $Na_2Fe(SO_4)_2$. The $Na_2Fe(SO_4)_2$ cathode shows a high Fe^{2+}/Fe^{3+} redox potential at ~3.6 V (vs. Na/Na^+), delivering 82 mAh g^{-1} at 0.1 C under nonoptimal carbon coating and exhibiting over 60% capacity retention at 2 C. Meanwhile, the cathode cycles stably with the capacity of 50 mAh g^{-1} and 83 mAh g^{-1} at 0.5 C at 0 °C and 55 °C respectively, showing superior electrochemical performance in broad operating temperature.

Experimental

Synthetic procedures

$Na_2Fe(SO_4)_2$ was prepared by reacting Na_2SO_4 and $FeSO_4$ at the molar ratio of 1:1 by solid reaction process in low temperature. The raw materials were mixed by ball milling at 400 rpm for 6h. After annealing the mixture in tubular furnace under steady argon flow at 200 °C for 12 h and then at 300~350 °C for 24 h, the pale-yellow target material was obtained. 20 wt % ascorbic acid was added to raw materials as carbon source and antioxidant to synthesize carbon-coated $Na_2Fe(SO_4)_2$. After the same ball-milling and annealing process, the black powder was obtained.

Material characterization

Elemental analysis was carried out using Inductively Coupled Plasma Optical Emission Spectrometry (ICP-OES, Optima 8000). The X-ray diffraction (XRD) patterns of our sodium iron sulfate samples were acquired by Bruker D8 diffractometer equipped with a Co-Kα radiation source (λ_1=1.78897 Å λ_2= 1.79285 Å). The structure were then refined with Rietveld method with the GSAS program. Typical scans were performed in 10~60 ° at the rate of 0.5 ° s^{-1} with the step size of 0.02 °. Temperature-controlled XRD was also carried out in the same diffractometer in air and N_2, repectively. Each pattern was recorded for ~10 min at a certain temperature between room temperature (~25 °C) and 650 °C. Room-temperature Mössbauer spectrum was measured with a ^{57}Co source in a Rh matrix using a Wissel-Mössbauer spectrometer, providing ^{57}Fe resonant radiation at 14.4 KeV. The X-ray photoelectron spectroscopy (XPS) was tested with an Escalab250Xi X-ray photoelectron spectrometer to reveal the valence state of Fe. Scanning electron microscopy (SEM, Hitachi SU70) and transmission electron microscope (TEM, FEI Tecnai G2 F20) were used to observe morphology and the microstructure of samples. The BET surface areas of samples were measured using nitrogen adsorption and desorption on a Micromertics Tristar II instrument. TGA/DSC was carried out between 50 °C and 650 °C in a constant flow of air and N_2, respectively, with a heating rate of 10 °C min^{-1}, using a simultaneous thermal analyzer TGA/DSC 3+.

Electrochemical characterization

Both the NFSO and NFSO/C cathodes were formulated by mixing 70 wt% active materials, 20 wt% Super P carbon black and 10 wt% polyvinylidene fluoride (PVDF) and then mixed uniformly by adding appropriate N-methyl-2-pyrrolidone (NMP). The resulting slurry was cast on an Al foil acting as current collector and dried at 120 °C in vacuum overnight. The mass loading of the electrode materials was about 2 mg cm^{-1}. The electrodes were transferred into a glovebox filled with argon, in which both moisture and oxygen levels were less than 1 ppm to assemble the coin-type cells (CR2025). Metallic sodium was used as the counter electrode. Cyclic voltammetry (CV) measurements were performed using a CHI660C electrochemistry work station at a scan rate of 0.1 mV s^{-1} within the potential range of 1.5~4.2 V (vs. Na/Na^+). The galvanostatic charge-discharge profiles were tested at a voltage ranging from 1.5 V to 4.2 V *vs.* Na/Na^+ on a Neware BTS-5 battery test system. The mass of active materials was calculated based on $Na_2Fe(SO_4)_2$ and the capacity of $Na_6Fe(SO_4)_4$ was deducted. Electrochemical impedance spectroscopy was conducted in the frequency ranging from 0.1 Hz to 1 MHz with an amplitude of 5 mV on an electrochemistry workstation (CHI604D).The hard carbon anode was prepared by mixing the same ratio of active materials, Super P carbon black and PVDF and through similar process and the mass loading of the hard carbon anode was about 0.5 mg cm^{-1}. After presodiation with metallic sodium as the counter electrode, the hard carbon anode was matched with the NFSO/C cathode to assemble the full cell and was tested at the voltage from 1.7 V to 4.1 V with the current density of 45 mA g^{-1}.

Results and discussion

$Na_2Fe(SO_4)_2$ (NFSO) was synthesized by a facile low-temperature solid-state method. Element analysis studied by ICP-OES (Table S1) and TEM-EDX (Fig. S1 and Table S2) verified that Na:Fe:S is very close to 2:1:2 in our samples. Its crystal structure was determined by XRD (Fig. 1a), which is found to be isostructural to alluaudite-type $Na_2Fe_2(SO_4)_3$. A Rietveld structure refinement using GSAS program is carried out,[26] resulting in a satisfactory fitting with R_{wp}=4.55% and R_p=3.04%. The atomic parameters of $Na_2Fe(SO_4)_2$ refined from XRD data are shown in Table S3. The lattice parameters increase slightly compared with $Na_{2+2x}Fe_{2-x}(SO_4)_3$ (x=0-0.4).[27] Minor amount of $Na_6Fe(SO_4)_4$ (~9.5% in molar fraction) as an impurity is detected in the analysis. Mössbauer spectrum (Fig. S2 and Table S4) was performed to study on the valence of Fe in NFSO samples and to verify the proportions quantitively further. Two doublets of equal intensity correspond to two Fe sites in NFSO, accounting for ~83.0% in total. The ~8.1% Fe^{2+} species correspond to $Na_6Fe(SO_4)_4$, which is in good agreement with the results of refinement. Meanwhile, there are ~8.9% Fe^{3+} doublet species existing, indicating only $Na_{2-x}Fe(SO_4)_2$ can be obtained originally due to the Na-rich impurity $Na_6Fe(SO_4)_4$. It should be noted that all Fe ions could be reduced to Fe^{2+} after the first discharging, resulting in the formation of Na-rich phase $Na_2Fe(SO_4)_2$ (XPS results shown in Fig. 3a). There may be some undetected minor phases existing allowing for mass balance. As shown in Fig. 1b and Fig. S3,† structure of NFSO is composed of Fe_2O_{10} dimer units connected by SO_4 tetrahedral that forms the typical alluaudite-type framework, in which sodium ions occupy three different kinds of sites. NFSO contains tunnels formed by the association of Fe_2O_{10} dimer unit and SO_4 tetrahedra along the c-axis, constructing the fast pathway for the diffusion of sodium ions located at Na(2) and Na(3) sites. However, sodium ions at Na(1) sites would be blocked off by the SO_4 tetrahedra, making them electrochemically inactive for sodium storage. The theoretical specific capacity of NFSO is calculated to be 91 mAh g^{-1} based on the

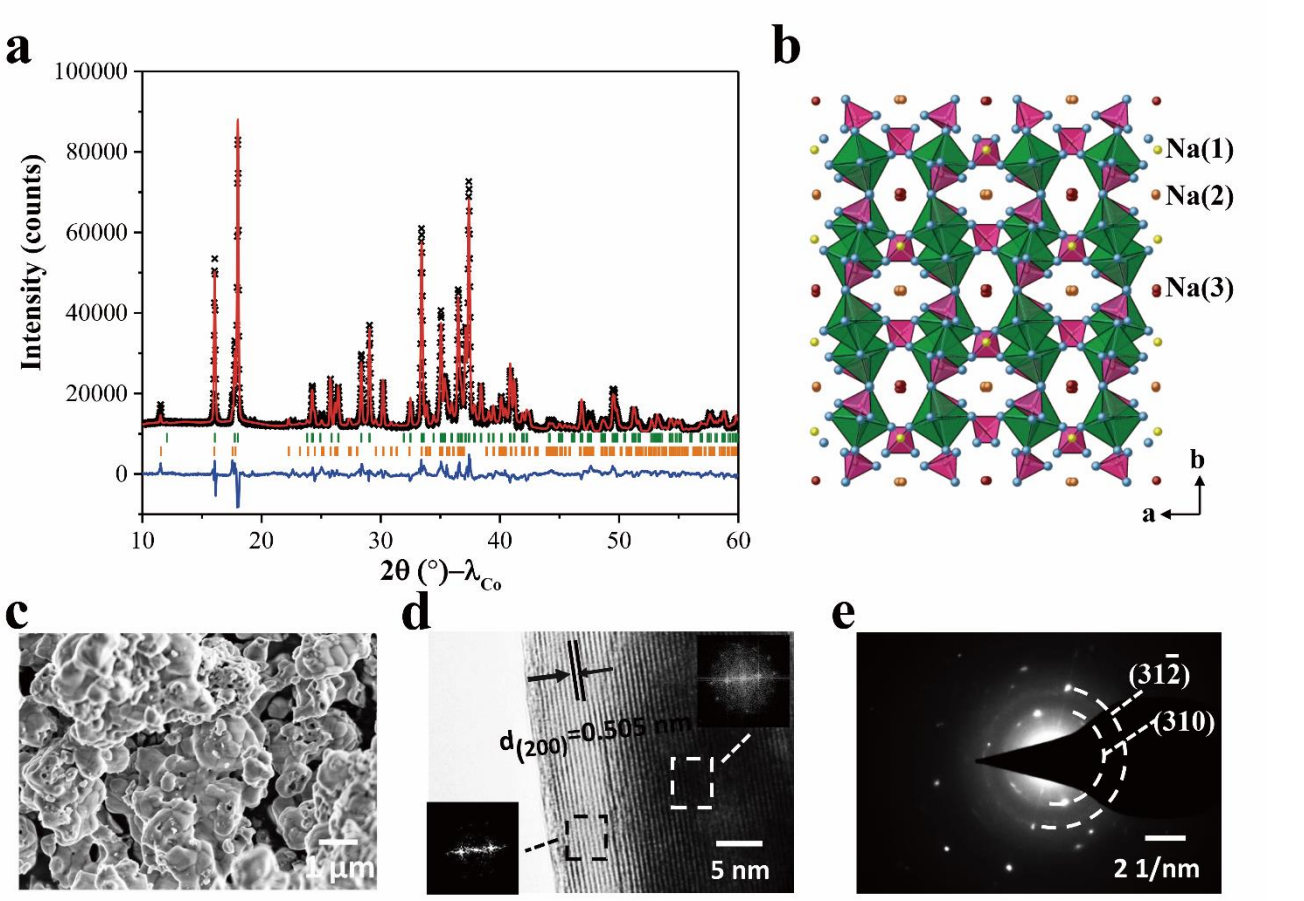

Fig. 1 (a) Rietveld refinement pattern of powder XRD data for $Na_2Fe(SO_4)_2$. Experimental data, calculated profile and their difference are shown as black crosses, red lines and blue lines. The theoretical Bragg positions are shown as green vertical lines. Minor amount (~9.5%) of $Na_6Fe(SO_4)_4$ as an impurity was included in analysis, shown as orange vertical lines. (b) The structure of $Na_2Fe(SO_4)_2$ along the c-axis. FeO_6 octahedra are green, SO_4 tetrahedra are pink and O atoms are blue. Na(1), Na(2) and Na(3) atoms are yellow, orange and red, respectively. (c) SEM image (d) HR-TEM image (e) SAED pattern of $Na_2Fe(SO_4)_2$.

full usage of sodium ions at Na(2) and Na(3) sites. Further inspection on NFSO using high-resolution TEM and more specifically from selected area electron diffraction (SAED) patterns are shown in Figure 1d-e. The (200) d-spacing of 0.505 nm is in well accordance with the peak at 17.96 ° in the XRD pattern. Moreover, the multi-crystal diffraction rings in the SAED pattern can be indexed using NFSO cell parameters determined from the XRD refinement, which are consistent with (31$\bar{2}$) and (310) plane respectively, indicating the accuracy of the indexing results.

It is worth noting that the electronic conduction in NFSO might be obstructed since Fe_2O_{10} dimers are separated from each other by SO_4 groups.[28] Accordingly, to introduce carbon coating in NFSO is necessary to get full use of sodium storage ability of NFSO.[29] Given the relatively low synthesis temperature of NFSO, ascorbic acid was mixed with other raw materials and sintered together *in-situ* forming a carbon layer as well as to prevent Fe^{2+} from oxidation. The morphologies of bare NFSO and NFSO/C were examined by SEM and TEM (Fig. 1c and Fig. S4†). Bare NSFO is made of agglomerates, while the NSFO/C is made of incompact particles with sizes of 0.5-1 μm that are wrapped by carbon layers, which is beneficial for electron transfer and mitigation of side reactions with electrolyte. The carbon content is about 10 wt% obtained from thermogravimetric analysis (TGA, Fig. S12†).

The electrochemical properties of NFSO/C were examined using CV and galvanostatic charge-discharge as shown in Fig. 2. Bare NFSO was also included in Fig. S5† for comparison. A series of redox peaks located at 3.02/2.78, 3.52/3.42, 3.75/3.67 and 4.05/3.78 V were recorded in CV curves of NFSO/C (Fig. 2a), in which the higher peaks over 3.4 V can be ascribed to the stepwise redox reactions of NFSO. The corresponding bare NFSO also exhibits the electrochemical activity over 3.4 V (Fig. S5†), but the pair of wide peaks with lower peak current suggest the insufficiently activated redox in bare NFSO due to the intrinsic poor electronic conduction. The pair of weak peaks at 3.02/2.78 V in the electrode of NFSO/C might be associated with the poor electrochemical activity of the minor impurity of $Na_6Fe(SO_4)_4$ as indicated in Fig. S6†. In consistent with the CV scans, the NFSO/C electrode exhibits a high average discharge potential of ~3.6 V and a close-to-theoretical capacity of 82 mAh g^{-1} featured by a sloping voltage profile, indicating single-phase solid solution mechanism without phase transformation evidenced by the latter *ex-situ* XRD analysis. Such a high redox potential not only results from the strong inductive effect of sulfate radical but also owes to Fe_2O_{10} dimer, formed by two FeO_6 octahedra sharing edge instead of sharing corner, which decreases the distance between two Fe ions and results in a reduced electric field and higher redox voltage.[15-17]

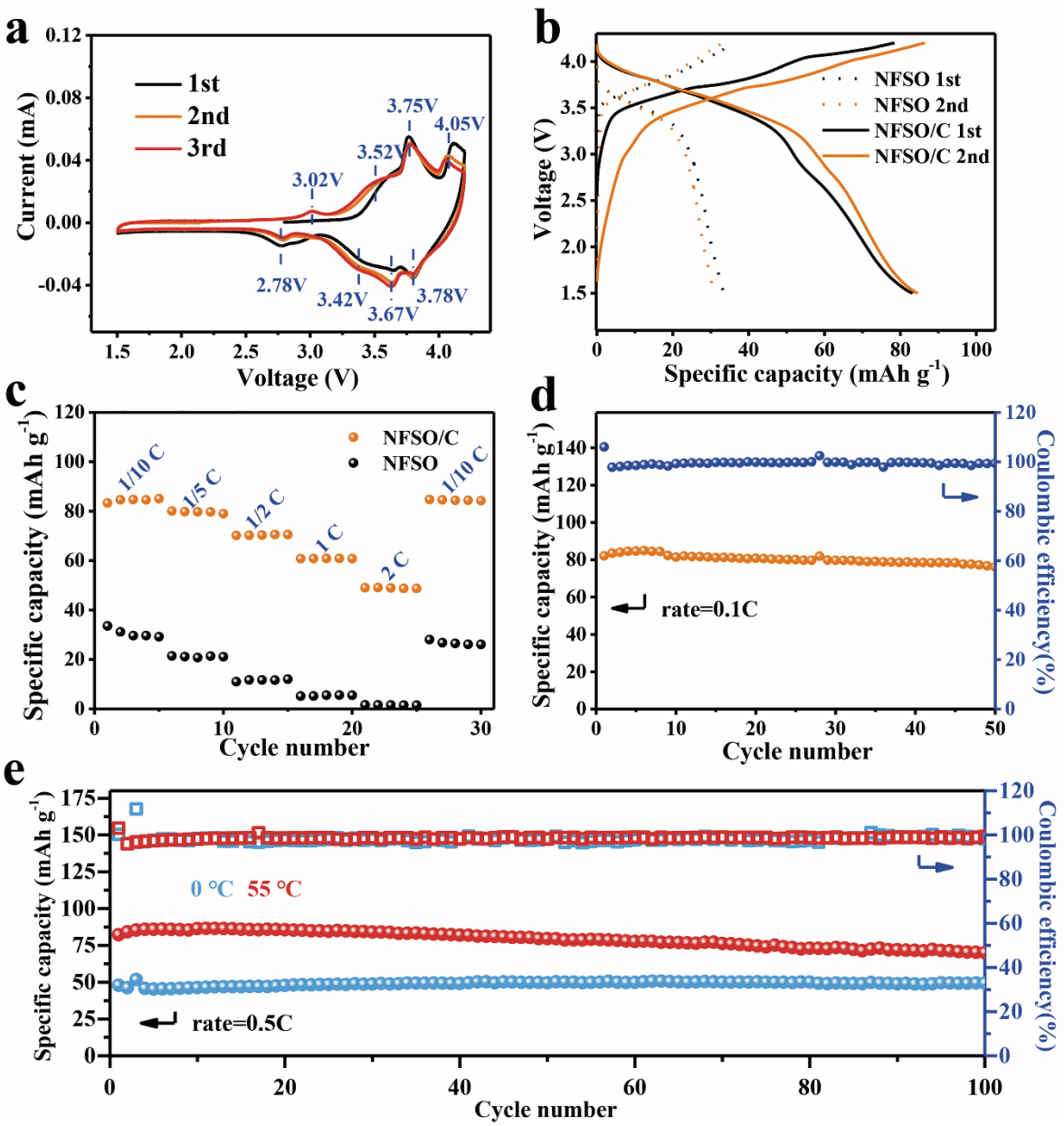

Fig. 2 (a) Cyclic voltammograms for the 1st to 3rd cycle for NFSO/C at a scan rate of 0.1 mV s^{-1}. (b) Galvanostatic charge–discharge profiles of NASO and NFSO/C at 0.1 C cycled between 1.5 V and 4.2 V. (c) Capacity retention of NFSO and NFSO/C upon cycling up to 30 cycles at various rate from 0.1 C to 2 C. (d) Cycling performance and Coulombic efficiency of NFSO/C at 0.1 C for 50 cycles. (e) Cycling performance of NFSO/C cathode at 0 °C and 55 °C and corresponding Coulombic efficiency.

Rate capability of NFSO/C and bare NFSO were evaluated at different rates from 0.1 to 2 C as shown in Fig. 2c. In contrast to the nearly zero capacity of bare NFSO at 2 C, the NFSO/C electrode maintains 50 mAh g^{-1} with over 60% capacity retention and recovers to 82 mAh g^{-1} when the rate returns back to 0.1 C. Furthermore, the NFSO/C electrode also exhibits superior cycling stability with nearly no capacity loss over 50 cycles. To further investigate the kinetics of NFSO and NFSO/C, electrochemical impedance spectroscopy (EIS) was carried out (Fig. S7†). Charge transfer resistance of NFSO/C (49.64 Ω) is much lower than that of NFSO (84.09 Ω), indicating a faster charge transfer process of NFSO/C. In addition, the diffusion coefficients of sodium were calculated based on EIS, the process and corresponding figure of which have been shown in ESI†, Fig. S8-9. The NFSO and NFSO/C eletrodes exhibit diffusion coefficients of sodium as 1.17×10^{-12} and 1.73×10^{-12} cm^2 s^{-1}, respectively. All these results above clearly indicate the superiority of NFSO in terms of sodium storage. To further explore the potentials of NFSO/C utilized in a wide temperature range for future applications, its electrochemical performance was respectively tested at 0 °C and 55 °C, characterized by electrochemical impedance spectroscopy (Fig. S10 †) and corresponding galvanostatic charge-discharge cycling (Fig. 2e). Although the charge transfer resistance of the electrode at 0 °C (350 Ω) is quite larger than that at 55 °C (33 Ω) due to the slow ion kinetics at low temperature, [30] a reversible capacity of 50 mAh g^{-1} can still be

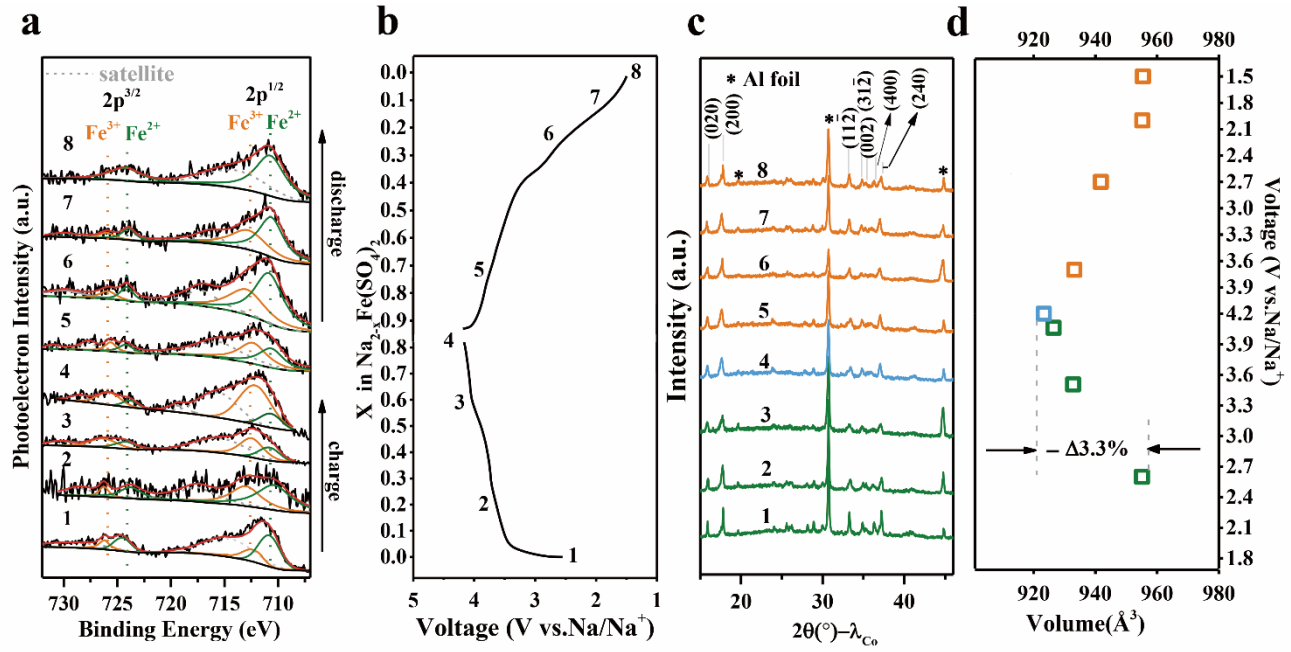

Fig. 3 (a) XPS Fe 2p narrow spectra of NFSO under different voltage states. (b) X in $Na_{2-x}Fe(SO_4)_2$/C -voltage curve under 0.1 C. (c) *Ex situ* XRD patterns of NFSO/C at different charge/discharge states. (d) Cell volumes at corresponding potentials.

achieved at 0 °C after 100 cycles, corresponding to a capacity retention of ~70% of that at room temperature. At high temperature of 55 °C, the electrode delivers 83 mAh g^{-1} at 0.5 C and exhibits a capacity retention of ~84% over 100 cycles.

To reveal the valence change of Fe and better understand the mechanism during sodium extraction and re-insertion process, XPS was carried out on certain voltage states of the first charge-discharge profiles (Fig. 3a,b). In the as-prepared electrode materials, most Fe ions exist in Fe^{2+}, yet a weak pair of Fe^{3+} peaks exist, which suggests sodium in our materials is not up to 2. During charging from OCV to 4.2 V, the Fe 2p peaks gradually shift to higher binding energy, indicating Fe^{2+} has been oxidized to Fe^{3+} along with sodium extraction. The area of Fe^{3+} peaks expand at 4.2 V but a small region of Fe^{2+} peaks still remains, which is probably due to a small amount of $Na_6Fe(SO_4)_4$. During discharging, the binding energy of Fe gradually shifts back to lower energy, representing the reduction of Fe^{3+} to Fe^{2+}. All of Fe ions have been reduced to Fe^{2+} at 1.5 V, showing

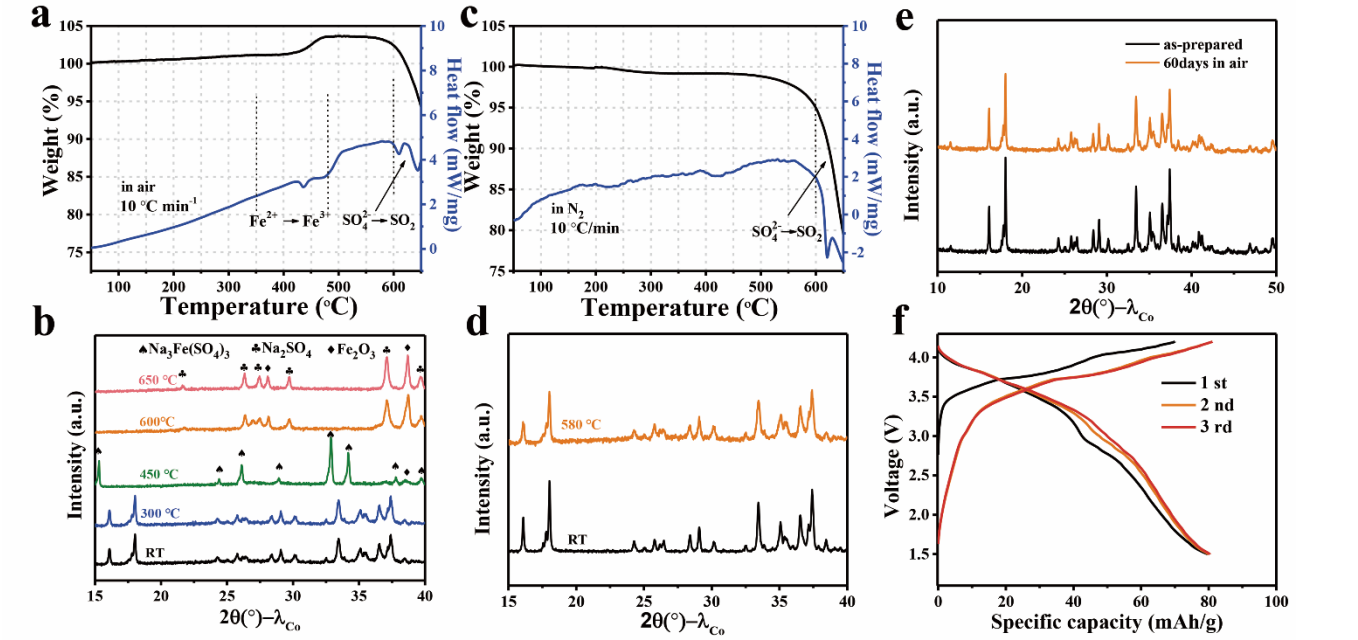

Fig. 4 TGA/DSC of NFSO at a rate of 10 °C min^{-1} (a) in air (b) in N_2. Temperature-controlled XRD of NFSO (c) in air (d) in N_2. (e) XRD patterns of the as-prepared NFSO/C and that exposed to air for 60 days. (f) Galvanostatic charge–discharge profiles of NFSO/C after exposed to air for 60 days at 0.1 C cycled between 1.5 V and 4.2 V.

high reversibility, corresponding to ~0.9 Na^+ re-insertion and ~3.6 V average potential.

Ex-situ XRD was also conducted to investigate the structural evolution of NFSO/C upon electrochemical cycling (Fig. 3c). The major peaks of XRD pattern almost do not shift, based on which the -3.3% of volume change has been confirmed. Compared with other polyanion compounds in volume change, such as $LiFePO_4$ (-6.9%) and $LiFeSO_4F$ (-10.4%), $Na_2Fe(SO_4)_2$ attains much higher structural stability, which is beneficial for long-term cycling.[17,20,21,31] The magnified graph (2θ=10~25 ° and 32~46 °) in Fig. S11† shows that, during charging, both the intensities of peaks corresponding to the (200) plane and the (400) plane gradually become weaker and shift slightly to the lower angles, which may be ascribed to Na^+ extraction and leading to increase of interplanar distance. We also notice that the $(11\bar{2})$ peak has split and the (002) peak has disappeared when charging to 4.1 V, which may be due to the disordered distribution of Na^+ to some extent. [32-34] The reserve peak variation can be observed during the subsequent discharge and all peaks shift back to the original sites and no volume change remains, showing the full reversibility of the NFSO/C cathode.

Despite possessing remarkable voltage, sulfate-based cathodes usually suffer from pyrogenic decomposition and moisture absorption.[17-21] Their poor thermal stability is mainly due to unstable sulfate radical being prone to decompose into SO_2 gas at low temperature (~450 °C), which not only causes severe deterioration in electrochemical properties but incurs safety concerns. The stability of NFSO was characterized by TGA/DSC and temperature-controlled XRD in both air and N_2 atmosphere (Fig. 4a-d). When heated in air from 50 °C to 650 °C, there are mainly three stages for the TGA curves of NFSO that can be observed. At ~450 °C, NFSO gains weight and an endothermic peak appears correspondingly, probably resulting from oxidation of Fe^{2+}. Surprisingly, when heated to higher temperature, TGA curves remain unchanged until 580 °C, which indicates the high thermal stability of sulfate radical. Temperature-controlled XRD in air reveals that $Na_2Fe(SO_4)_2$ would initially transform into $Na_3Fe(SO_4)_3$ along with minor formation of Fe_2O_3 at 450 °C and further decompose into Na_2SO_4 and Fe_2O_3 at 600 °C. Therefore, it is reasonable to infer that sulfate radical in NFSO can keep stable at the high temperature of 580 °C even though Fe^{2+} has been oxidized at 450 °C. Given that no oxygen exists in batteries, N_2 was used to

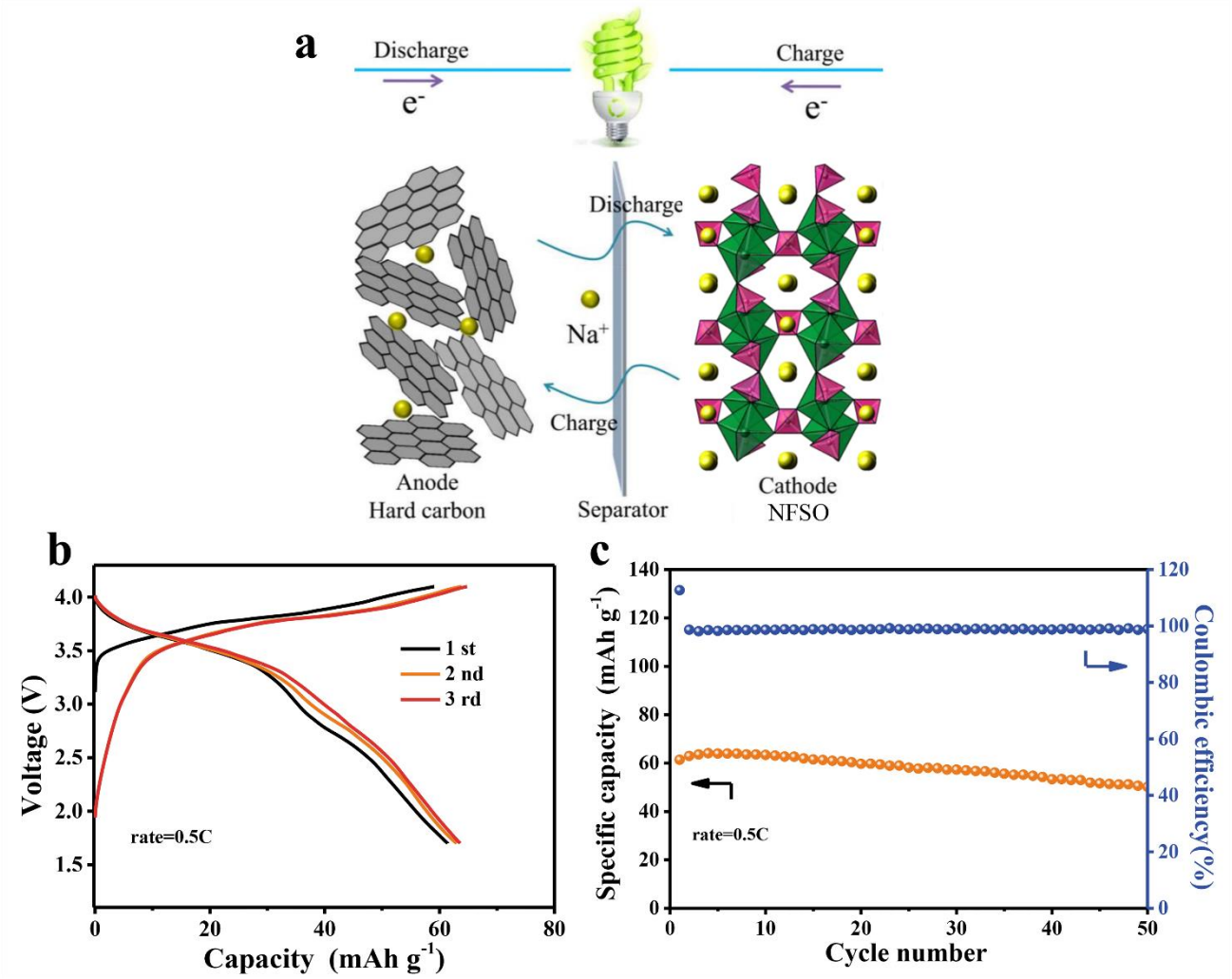

Fig. 5 (a) Schematic illustration of the full cell with NFSO/C as the cathode and the hard carbon as the anode. (b) Discharge/charge profiles (c) cycling performance of full cell.

provide more similar atmosphere for NFSO to further explore the thermal stability. Since no obvious weight of NFSO changes until 580 °C and all peaks in XRD pattern remain alike as well, it is clear that our NFSO exhibits a high thermal stability up to 580 °C, which is of great advantage in contrast to the previously reported SO_4-based electrode materials.

Apart from thermal stability, the moisture resistance capability of sulfates is also of crucial importance because high absorption of water may destroy the structure of materials and cause the side reactions between electrolyte and electrode, which affects cycling performance and limits the application. To investigate the hygroscopicity of our sulfates, the NFSO/C powder was laid in air for 60 days. After that, its structure and electrochemical performance were measured by XRD and galvanostatic charge-discharge cycling, which were shown in Fig. 4e-f. All the peaks of XRD pattern are almost alike with that in the fresh NFSO, indicating no sulfate hydrate forms. Therefore, the sodium diffusion pathways stay quite stable, resulting in nearly the same voltage slope and capacity as the fresh materials.

To further investigate the NFSO/C cathode in practical application, full cell was assembled with hard carbon (HC) anode after presodiation (Fig. S13†) at 45 mA g^{-1} in advance and measured by galvanostatic charge-discharge cycling at the rate of 0.5 C (45mA g^{-1}) in the voltage window of 1.7~4.1 V. As shown in Fig. 5a-c, the full cell can deliver 65 mAh g^{-1} with the operating voltage of 3.3 V, of which the corresponding energy density is 171.6 Wh kg^{-1} (based on the total mass of cathode and anode active materials) and the Coulombic efficiency is ~99.1% except for the first cycle. Though the specific capacity of our NFSO/C cathode is relatively low, its high operating voltage guarantees the full cell a promising energy density.

Conclusions

An alluaudite-type sulfate cathode $Na_2Fe(SO_4)_2$ combining outstanding thermal stability and favorable moisture-resistant property was synthesized by low-temperature solid method. It exhibits a high Fe^{2+}/Fe^{3+} redox potential at ~3.6 V (*vs.* Na/Na^+), which delivers 82 mAh g^{-1} at 0.1 C under nonoptimal carbon coating and exhibits over 60% capacity retention at 2 C. Meanwhile, the cathode cycles stably with the capacity of 50 mAh g^{-1} and 83 mAh g^{-1} at 0.5 C at 0 °C and 55 °C respectively. Notably, the high thermal stability (580 °C) and superior moisture resistance (60 days in air) make $Na_2Fe(SO_4)_2$ outstanding in comparison with the previously reported SO_4^{2-}-based electrode materials. Our work offers great potentials for investigating more high voltage, good safety and low-cost sulfate cathode materials for rechargeable batteries.

Conflicts of interest

There are no conflicts to declare.

Acknowledgements

This work is supported by National Natural Science Foundation of China (Grant No. 51722105), National key research and development program (Grant No. 2016YFB0901600), Zhejiang Provincial Natural Science Foundation of China (LR18B030001), and the Fundamental Research Funds for the Central Universities (2018XZZX002-08).

*Corresponding Author - yzjiang@zju.edu.cn

References

1 B. Scrosati, J. Hassoun, Y.-K. Sun, *Energy Environ. Sci.,* 2011, **4**, 3287.
2 V. Etacheri, R. Marom, R. Elazari, G. Salitra, D. Aurbach, *Energy Environ. Sci.,* 2011, **4**, 3243.
3 J.-M. Tarascon, *Nat. Chem.,* 2010, **2**, 510.
4 S.-C. Park, Y.-M. Kim, Y.-M. Kang, K.-T. Kim, P. S. Lee, J.-Y. Lee, *J. Power Sources,* 2001, **103**, 86.
5 S. Kang, S. Kang, K. Ryu, S. Chang, *Solid State Ionics,* 1999, **120**, 155.
6 J. B. Goodenough, A. Manthiram, *MRS Commun.,* 2014, **4**, 135.
7 R. Chen, R. Luo, Y. Huang, F. Wu, L. Li, *Adv. Sci.,* 2016, **3**, 1600051.
8 B. Dunn, H. Kamath, J.-M. Tarascon, *Science,* 2011, **334**, 928.
9 N. Yabuuchi, K. Kubota, M. Dahbi, S. Komaba, *Chem. Rev.,* 2014, **114**, 11636.
10 Y. Fang, Z. Chen, L. Xiao, X. Ai, Y. Cao, H. Yang, *Small,* 2018, **14**, 1703116.
11 A. K. Padhi, K. S. Nanjundaswamy, J. B. Goodenough, *J. Electrochem. Soc.,* 1997, **144**, 1188.
12 A. Yamada, S.-C. Chung, K. Hinokuma, *J. Electrochem. Soc.,* 2001, **148**, A224.
13 Y.-H. Huang, J. B. Goodenough, *Chem. Mat.,* 2008, **20**, 7237.
14 J.-Y. Hwang, S.-T. Myung, Y.-K. Sun, *Chem. Soc. Rev.,* 2017, **46**, 3529.
15 A. Padhi, K. Nanjundaswamy, C. Masquelier, S. Okada, J. Goodenough, *J. Electrochem. Soc.,* 1997, **144**, 1609.
16 A. Gutierrez, N. A. Benedek, A. Manthiram, *Chem. Mat.,* 2013, **25**, 4010.
17 P. Barpanda, G. Oyama, S.-i. Nishimura, S.-C. Chung, A. Yamada, *Nat. Commun.,* 2014, **5**, 4358.
18 M. Reynaud, G. Rousse, A. M. Abakumov, M. T. Sougrati, G. Van Tendeloo, J.-N. Chotard, J.-M. Tarascon, *J. Mater. Chem. A,* 2014, **2**, 2671.
19 P. Barpanda, G. Oyama, C. D. Ling, A. Yamada, *Chem. Mat.,* 2014, **26**, 1297.
20 L. Lander, M. Reynaud, G. l. Rousse, M. T. Sougrati, C. Laberty-Robert, R. J. Messinger, M. l. Deschamps, J.-M. Tarascon, *Chem. Mat.,* 2014, **26**, 4178.
21 N. Recham, J.-N. Chotard, L. Dupont, C. Delacourt, W. Walker, M. Armand, J.-M. Tarascon, *Nat. Mater.,* 2010, **9**, 68.
22 Y. Lu, L. Wang, J. Cheng, J. B. Goodenough, *Chem. Commun.,* 2012, **48**, 6544.
23 Y. Jiang, S. Yu, B. Wang, Y. Li, W. Sun, Y. Lu, M. Yan, B. Song, S. Dou, *Adv. Funct. Mater.,* 2016, **26**, 5315.
24 B. Wang, Y. Han, X. Wang, N. Bahlawane, H. Pan, M. Yan, Y. Jiang, *iScience,* 2018, **3**, 110.
25 S. Lux, I. Lucas, E. Pollak, S. Passerini, M. Winter, R. Kostecki, *Electrochem. Commun.,* 2012, **14**, 47.

26 B. H. Toby, *J. Appl. Crystallogr.,* 2001, **34**, 210.
27 G. Oyama, S. Nishimura, Y. Suzuki, M. Okubo, A. Yamada, ChemElectroChem, 2015, **2**, 1019–1023.
28 C. Masquelier, L. Croguennec, *Chem. Rev.,* 2013, **113**, 6552.
29 X. Xiang, K. Zhang, J. Chen, *Adv. Mater.,* 2015, **27**, 5343.
30 Y. Qiao, J. Tu, X. Wang, C. Gu, *J. Power Sources,* 2012, **199**, 287.
31 P. Moreau, D. Guyomard, J. Gaubicher, F. Boucher, *Chem. Mat.,* 2010, **22**, 4126.
32 Z. Ye, X. Zhao, S. Li, S. Wu, P. Wu, M. C. Nguyen, J. Guo, J. Mi, Z. Gong, Z.-Z. Zhu, *Electrochim. Acta,* 2016, **212**, 934.
33 S. Li, J. Guo, Z. Ye, X. Zhao, S. Wu, J.-X. Mi, C.-Z. Wang, Z. Gong, M. J. McDonald, Z. Zhu, *ACS Appl. Mater. Interfaces,* 2016, **8**, 17233.
34 W. Guan, B. Pan, P. Zhou, J. Mi, D. Zhang, J. Xu, Y. Jiang, *ACS Appl. Mater. Interfaces,* 2017, **9**, 22369.

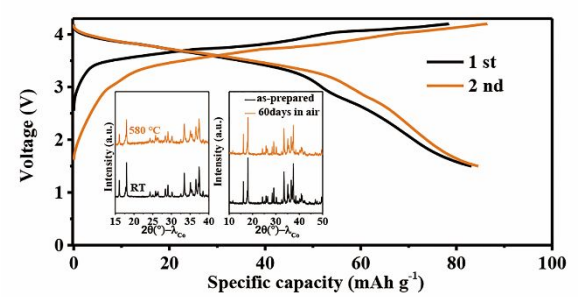

A new high-voltage earth-abundant cathode for sodium-ion battery, $Na_2Fe(SO_4)_2$, is reported, combining with high thermal stability and good moisture resistance.